JACS
JOURNAL OF THE AMERICAN CHEMICAL SOCIETY
pubs.acs.org/JACS
Article

Chemically Spiraling $CsPbBr_3$ Perovskite Nanorods

Suman Bera, Sanjib Shyamal, and Narayan Pradhan*

Cite This: J. Am. Chem. Soc. 2021, 143, 14895−14906
Read Online
ACCESS | Metrics & More | Article Recommendations | Supporting Information

ABSTRACT: Light emitting lead halide perovskite nanocrystals are currently emerging as the workhorse in quantum dot research. Most of these reported nanocrystals are isotropic cubes or polyhedral; but anisotropic nanostructures with controlled anisotropic directions still remain a major challenge. For orthorhombic $CsPbBr_3$, the 1D shaped nanostructures reported are linear and along either of the axial directions ⟨100⟩. In contrast, herein, spiral $CsPbBr_3$ perovskite nanorods in the orthorhombic phase are reported with unusual anisotropy having (101) planes remaining perpendicular to the major axis [201]. While these nanorods are synthesized using the prelattice of orthorhombic Cs_2CdBr_4 with Pb(II) diffusion, the spirality is controlled by manipulation of the compositions of alkylammonium ions in the reaction system which selectively dissolve some spiral facets of the nanorods. Further, as spirality varied with facet creation and elimination, these nanorods were explored as photocatalysts for CO_2 reduction, and the evolution of methane was also found to be dependent on the depth of the spiral nanorods. The entire study demonstrates facet manipulation of complex nanorods, and these results suggest that even if perovskites are ionic in nature, their shape could be constructed by design with proper reaction manipulation.

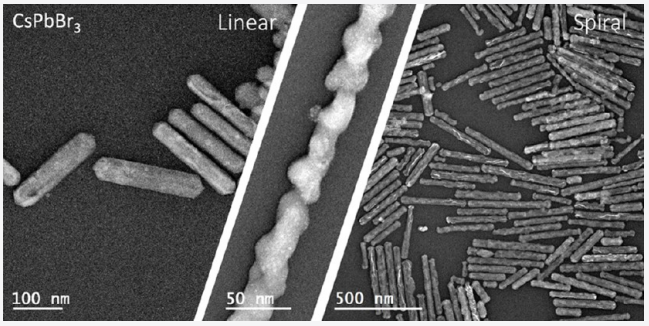

INTRODUCTION

Lead halide perovskite nanocrystals have recently emerged as a leading optical material in current research.[1−8] Significant successes have been achieved in their synthesis and understanding of their formation chemistry.[5,8−19] However, due to their ionic character and very fast formation, the growth kinetics of these nanocrystals in high temperature solution processed methods could not yet be established. This indeed created hurdles for their wide synthesis exploration and obtaining as desired dimensions or controlling the facet directive anisotropic growth. This narrowed down the advance synthesis pathways for dimension modulations of these highly important materials in comparison to widely established chalcogenides or metal oxides. There are reports on slowing down reactions and formulating kinetics parameters;[20−22] but there is no evidence established yet on the mechanism of their shape or size transformation from one to another size domain. Hence, the synthesis and discovery of new chemistry for nanocrystal shape modulations still remains open and more fundamental understandings are required for establishing the same.

For investigating more on chemical processes related to nanocrystals fabrications, different synthetic reports on lead halide perovskite nanocrystals are analyzed and it is revealed that almost all reports on the high temperature synthesis largely followed the procedure developed by Kovalenko and co-workers in 2015.[1] Understanding the reaction system, several modifications on ligands, precursors, and reaction temperature are further carried out.[2,8,17,23,24] Among these benzoyl bromide,[25] *N*-bromosuccinimide,[26] oleylammonium bromide,[27] and some other halide sources[22,28,29] are efficiently used for obtaining the cube shapes of these nanocrystals. In another modification, phenacyl bromide, an α-halo ketone, was also used; but these stabilized polyhedral shapes were different from cube nanocrystals and helped in modulating the shape architectures of these nanocrystals.[30]

Beyond these, several ligands are also developed and implemented for surface capping of these nanocrystals.[9,10,31−38] While ligands help with facet stabilization and the halide sources control the versatility of their synthesis as well as provide halide sufficient environment for obtaining bright emission,[39−42] the core issue of control over the formation of the crystal lattice of these nanocrystals still remains unclear. There is no convincing data reported yet on the direct one to one precursor's reaction and the control of their nucleation followed by successive growth as expected in the classical approach. A closer look at the different reactions reveals that the formation of these lead halide perovskite nanocrystals follows some equilibrium processes. These might

Received: July 13, 2021
Published: September 1, 2021

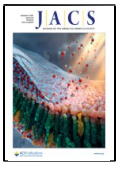

https://doi.org/10.1021/jacs.1c07231
J. Am. Chem. Soc. 2021, 143, 14895−14906

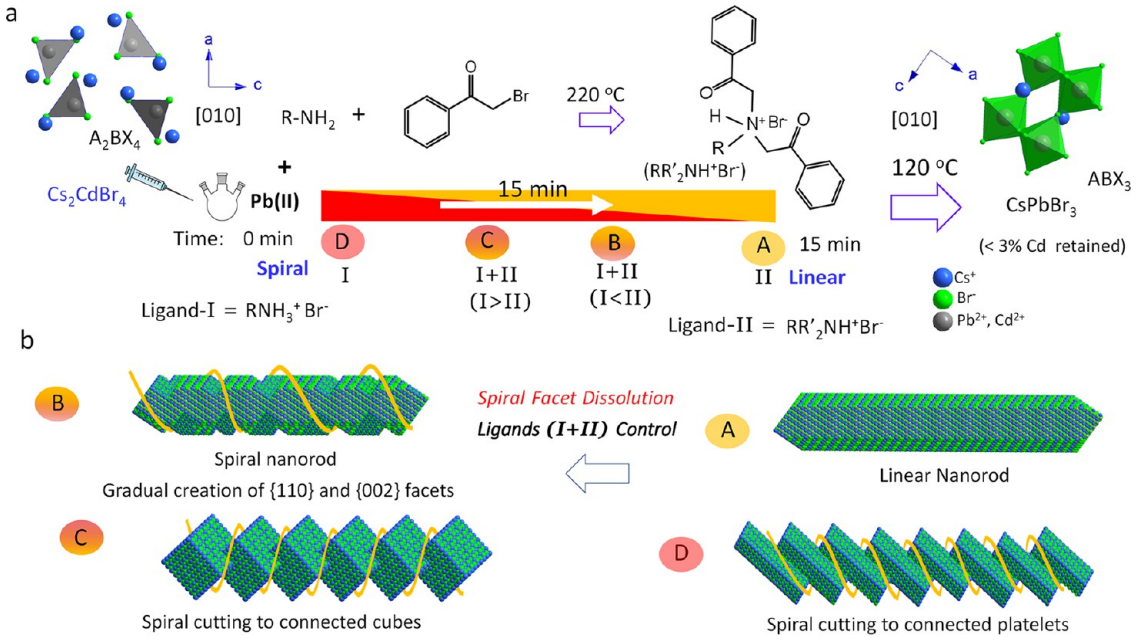

Figure 1. (a) Schematic presentation of transformation of orthorhombic Cs_2CdBr_4 to same phase $CsPbBr_3$ nanorods. The reaction shows the progress of formation of tertiary ammonium bromide from the reaction of oleylamine with phenacyl bromide where initial mixture of oleylammonium bromide (Ligand-I) transformed to corresponding tertiary ammonium bromide (Ligand-II) within a period of 15 min at 220 °C. A_2BX_4 and ABX_3 are the composition of the parent crystal and the product, respectively. Atomic models are shown along respective [010] views of both halides. A, B, C, and D are four conditions marked during the progress of reactions having mixture as well as dominated product of primary and tertiary ammonium bromides. (b) Models showing $CsPbBr_3$ nanorods spirally cutting to different spiral nanorods with different reaction conditions of A to D. For the case of C, models are done with normal cubes though truncated shaped were observed. All these models are schematic and were designed using Diamond Crystal Impact software. Cs atoms in all cases were kept on surfaces.

be precursor related or with amine/acid reactants in the reaction systems.[8,40,43,44] Sometimes, these equilibria led to non-perovskite halides; and in the case of $CsPbBr_3$, these remained Cs_4PbBr_6 and $CsPb_2Br_5$.[8,33,40,43−47] Recent reports suggest that all these lead halides were transformed from one to another and share similar Cs atomic placements in their lattice structures.[48,49] Recently, it was also reported that Cs_2ZnBr_4 can extend its lattice for ion diffusion and formation of $CsPbBr_3$ nanocrystals.[50] These methods where either Cs_4PbBr_6 or CsBr or Cs_2ZnBr_4 were used as the starting material to extend their lattices, finally generating $CsPbBr_3$ perovskite nanocrystals by Pb(II) insertions. Moreover, the greatest advantage in this conversion is the shape modulation, which could be designed simply by architecting the parent nanostructures whether isotropic or anisotropic in nature. Further, this approach also sheds light on formulating the advance synthesis of complex nanostructures beyond simple linear, disc, or polyhedron nanocrystals. However, questions arise as to what could the new reagents be and how to select them to bring about new shapes in perovskite nanocrystals. As stated, benzoyl bromide and phenacyl bromide, which only differ in one carbon (−CH_2−), can behave differently and change the surface facets of the resulting nanocrystals drastically. Hence, there might be some closely related reagents in terms of composition, but these could lead to new nanostructures.

To address this, while searching for new reagents and new parent nanocrystals, Cd(II) remained the first choice as it has the ability to form tetrahedra as well as octahedra with halides,[51−53] and can also reside inside the lead halide perovskite lattice. There are reports on Cd(II) doping and Cd(II) as a major component in lead halide perovskite nanocubes as well as in nanorods.[41,52−54] However, with benzoyl bromide, it led to hexagonal $CsCdBr_3$;[54] but the composition, phase, and shape changed to orthorhombic Cs_2CdBr_4 while reacting with phenacyl bromide. With this turning point, herein, Cd(II) was explored for designing anisotropic parent nanocrystals which behaved differently from all such reports and led to spiral nanorods after Pb(II) introduction. This became a new synthesis modulation by design and became unique in perovskites, and also for all kinds of inorganic nanostructures. This was possible as the resulting $CsPbBr_3$ perovskite nanorods obtained had [201] anisotropy in contrast to all reports where ⟨100⟩ was only observed along the major axis.[50,55−63] Further, using the mixture of ligands and controlling reaction parameters, the spirality of these nanorods were also modulated. This was related to the ligand-induced selective surface binding and dissolution of unfavorable facets in a spiral manner, and led to depth variable spiral nanorods. As the spirality varied with reaction conditions, surface facets also varied. Hence, these nanorods were further explored for adsorption induced photocatalysis for reduction of CO_2, and a catalytic trend for methane evolution was observed to be dependent on the nature of the spirality of the nanorods. Details of the synthesis of different spiral nanorods, their characterizations, and the catalysis studies are carried out and reported in this article.

EXPERIMENTAL SECTION

Materials. Lead(II) oxide (PbO, 99.999%), cadmium oxide (CdO, 99.5%), cesium carbonate (Cs_2CO_3, reagent Plus, 99%), phenacyl bromide ($C_6H_5COCH_2Br$, 98%), oleic acid (OA, 90%), 1-octadecene (ODE, technical grade, 90%), oleylamine (OLA, 70%), ethyl acetate (EtOAc, anhydrous, 99.8%), chloroform-d ($CDCl_3$, 99.8%), and fluorine-doped tin oxide (FTO) were purchased from Sigma-Aldrich.

https://doi.org/10.1021/jacs.1c07231
J. Am. Chem. Soc. 2021, 143, 14895−14906

Tetrabutylammonium hexafluorophosphate ($TBAPF_6$) was purchased from TCI Chemicals. Solvents are purchased from Finer India. All chemicals were used without any further purification.

Methods. *Preparation of Cs-Oleate Stock Solution.* Cs-oleate solution was prepared following literature reported method.[1] In a typical synthesis, 1.2 mmol (390 mg) of Cs_2CO_3 and 2 mL of OA were taken in a three-neck round-bottom flask along with 18 mL of ODE, purged with nitrogen for 1 h at 120 °C, and then the temperature was increased to 150 °C for obtaining a clear Cs-oleate solution. This was further annealed for another 10 min, and then the solution was collected under hot conditions and stored in deaerated vial. Since Cs-oleate solidified at room temperature, it was preheated to 80 °C before using in the reactions.

Synthesis of Cs_2CdBr_4 Nanorods. Cesium cadmium bromide nanorods were synthesized by injection of Cs-oleate into a mixture of Cd-precursor, OA, OLA, and phenacyl bromide following a hot-injection protocol. In a typical synthesis, 0.2 mmol of CdO (25.6 mg), 0.6 mmol of phenacyl bromide (119.4 mg), 1 mL of OA, and 5 mL of ODE were loaded in a 25 mL round bottomed flask and deaerated at 120 °C for 1 h by purging nitrogen gas. Then the temperature was raised to 220 °C and 0.5 mL OLA was injected. The solution became red initially, then orange, and finally yellow with 15 min of annealing. After that, the temperature was decreased to 120 °C and 0.5 mL of Cs-oleate solution was swiftly injected into the yellow solution and annealed for 3 min. Finally, the reaction was ice quenched by dipping the reaction flask in an ice−water bath. These nanocrystals were further centrifuged at 3000 rpm for 5 min and precipitated nanocrystals were redispersed in deaerated octadecene (1 mL) for further use.

Synthesis of $CsPbBr_3$ Nanorods. $CsPbBr_3$ nanorods were synthesized by injecting Cs_2CdBr_4 nanorods solution in the reaction mixture containing Pb(II), phenacyl bromide along with OA and OLA. With different annealing times, the obtained nanorods were labeled as A, B, C, and D as presented in Figure 1. In a typical synthesis, 0.2 mmol of PbO (44 mg), 0.6 mmol of phenacyl bromide (119.4 mg), 1 mL of OA, and 5 mL of ODE were loaded in a 25 mL round bottomed flask and deaerated at 120 °C for 1 h by purging nitrogen gas. Then, the temperature was raised to 220 °C and 0.5 mL OLA was injected and annealed. The solution initially turned red to orange and then yellow within 15 min. For preparing nanorods-A, after 15 min annealing while the solution was yellow color (see Figure S1 of the Supporting Information, SI), the reaction was cooled down to 120 °C. Then, the stock of 1 mL Cs_2CdBr_4 nanorods solution was injected and annealed for 5 min and the reaction was ice-quenched for obtaining $CsPbBr_3$ nanorods-A.

For obtaining nanorods-B, -C, and -D, their respective annealing times were 8, 3, and 1 min after OLA injection, respectively, and all other procedures remained the same as for nanorods-A discussed above.

Purification. For harvesting the $CsPbBr_3$ nanocrystals, crude samples were taken in a centrifuge tube and as synthesized nanocrystals were separated from the reaction mixture by centrifugation at 3000 rpm for 5 min supernatant was discarded and the precipitated nanocrystals were redispersed in hexane for further characterisations.

Photocatalytic CO_2 Reduction. Photoreduction of CO_2 was carried out in a closed glass shell reactor in CO_2 saturated ethyl acetate and water mixture. In a typical procedure, 10 mL of ethyl acetate and water (300:1, v/v) mixture was taken in the glass shell reactor and heated to 120 °C for 2 min in order to form solid vapor interface. After cooling down to room temperature, approximately 5 mg of the $CsPbBr_3$ nanorod photocatalysts in 1 mL ethyl acetate were introduced into the glass shell reactor. Then, CO_2 gas was purged to 1 bar initially for 30 min to remove other contained gases and further continued to another 30 min for saturation. A 450 W Xe arc lamp with a calibrated intensity of 150 mW/cm^2 served as the light source during the photocatalytic measurements. The online gas chromatograph was connected to the reactor and the product generated during the measurements were analyzed with thermal conductivity detector (TCD) and flame ionization detector (FID) in a series with a fixed time interval of 30 min.

Photoelectrochemical (PEC) Measurement. For PEC measurements, purified nanorods were drop casted on FTO coated glass substrate and dried in an oven at 60 °C for 8h to form photoelectrodes. An electrochemical workstation with a standard three electrodes configuration was used for PEC measurements, where $CsPbBr_3$/FTO thin film was used as working electrode, Pt wire as counter one, and saturated Ag/AgCl as reference electrode. The electrodes were exposed to the 0.1 M tetrabutylammonium hexafluorophosphate ($TBAPF_6$)-ethyl acetate electrolyte through an O-ring with working surface area of 0.27 cm^2. Chronoamperometric I-t measurements were carried out at a fixed potential of −0.4 V vs Ag/AgCl under 100 mW/cm^2 chopped light illumination, and the electrochemical impedance spectroscopy (EIS) measurements were performed within the frequency range of 100 kHz to 100 mHz under illuminated conditions with an AC amplitude of 10 mV.

Instrumentation and Sample Preparation. UV−vis Spectra and Photoluminescence (PL) Spectra. UV−vis absorption spectra were collected with Agilent-Cary 60 UV−vis spectrophotometer and PL spectra were measured using a Horiba JobinYvon Fluoromax-4 spectrofluorometer. These spectra were measured by taking purified samples dispersed in hexane.

PL Quantum Yields (PLQY) and Time Correlated Single Photon Counting (TCSPC) Spectra. Photoluminescence quantum yield of the nanocrystals were recorded in Quanta Phi connected with Horiba JobinYvon Fluoromax-4 spectrofluorometer and the time correlated single photon counting (TCSPC) measurements were recorded using a Horiba Delta flex-01 TCSPC spectrometer. For the measurements, all solutions were diluted to an optical density of 0.1 or lower for minimizing the reabsorbance of the fluorophore. For the TCSPC measurements, the excitation wavelength was 402 nm, and the decays were measured at 518 nm.

Transmission Electron Microscopy (TEM) and High-Resolution TEM (HRTEM). TEM and HRTEM images were taken on a JEOL-JEM-F200 electron microscope with an accelerating voltage of 200 kV. Energy-dispersive spectroscopic (EDS) measurements were also performed on the same instrument. For the microscopic analysis, specimens were prepared by placing a drop of the purified nanocrystal solution in hexane on a carbon coated Cu-grid (300 mesh) purchased from Ted Pella and drying in the air and stored the grids in vacuum desiccator.

Powder X-ray Diffraction Measurement (XRD). Powder XRD was performed in a Bruker Advance D8 diffractometer, using Cu Kα (λ = 1.54 Å) as the incident radiation. For the XRD measurements, samples were prepared by drop casting a film of the nanocrystals on glass slides from the solution of nanocrystal dispersed in hexane.

^{1}H Nuclear Magnetic Resonance Spectroscopy (^{1}HNMR). ^{1}HNMR spectra were recorded on the Bruker DPX-500 spectrometer at room temperature by dispersing purified nanocrystals in $CDCl_3$.

Gas Chromatography (GC), Light Source, and Electrochemical Workstation for PEC. A 450 W Xe arc lamp from Newport with calibrated intensity 150 mW/cm^2 served as light source during the catalytic measurements. The gaseous products were detected by TRACE 1110, Thermo Scientific online gas chromatograph using thermal conductivity detector (TCD) and flame ionization detector (FID) in a series. Biologic, SP 300 workstation was used for the electrochemical measurement.

RESULTS AND DISCUSSION

For the synthesis of spiral $CsPbBr_3$ perovskite nanorods, the prelattice of a parent material Cs_2CdBr_4 was explored for Pb(II) insertion. Hence, the synthesis process was followed in two steps; first orthorhombic phase Cs_2CdBr_4 nanorods were synthesized and then, in the second stage, these nanorods were injected into the Pb(II) reaction system for obtaining the desired nanostructures. Phenacyl bromide and oleylamine reaction system[30] which supplied both halides and ligands were explored here in both steps for the formation of Cs_2CdBr_4 and

https://doi.org/10.1021/jacs.1c07231
J. Am. Chem. Soc. 2021, 143, 14895−14906

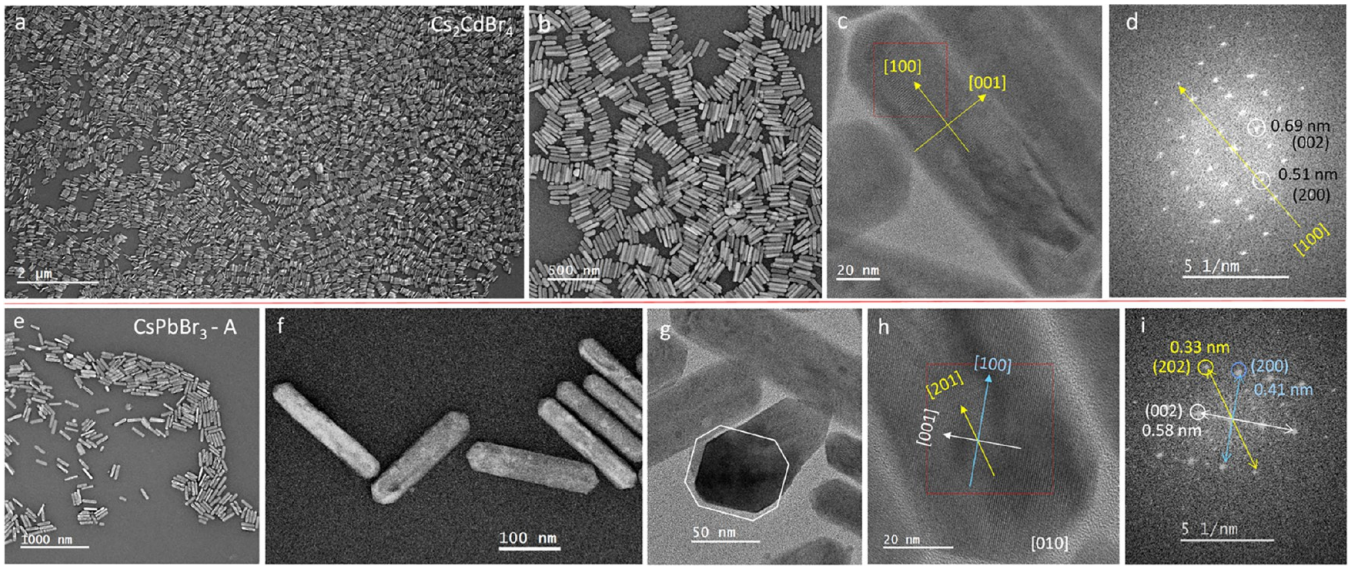

Figure 2. (a, b) Inverted TEM images of Cs_2CdBr_4 nanorods in different resolutions. (c) HRTEM image of a single nanorod of Cs_2CdBr_4. (d) Selected area FFT pattern showing the length direction as [100] of the orthorhombic phase. (e, f) Inverted TEM images of $CsPbBr_3$ in different resolutions obtained on reaction condition of A of Figure 1. (g) TEM imaging showing a vertically tilted nanorod. (h) HRTEM of $CsPbBr_3$ nanorod and (i) corresponding selected area FFT pattern showing the anisotropic direction as [201].

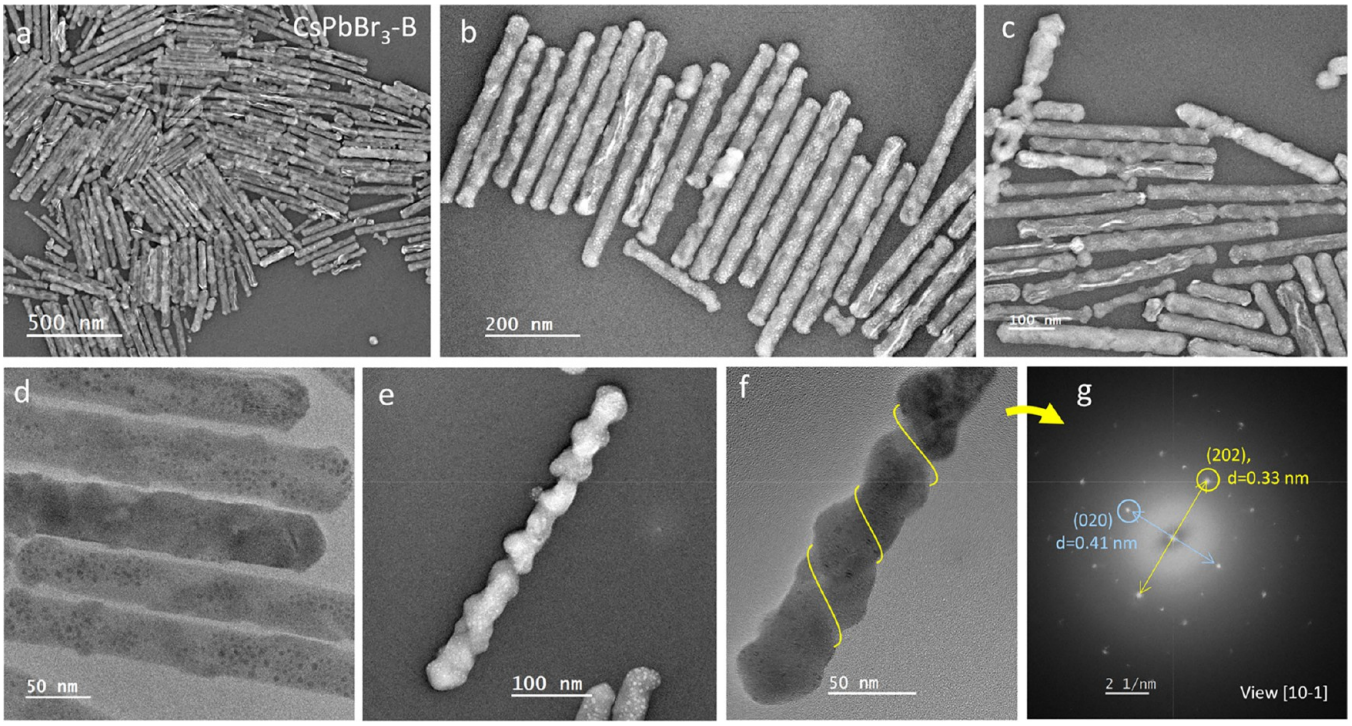

Figure 3. (a–c) Inverted TEM images of $CsPbBr_3$ spiral nanorods in different resolutions obtained on reaction condition of B of Figure 1. (d) Magnified TEM image of nanorods showing spirality. (e, f) Inverted TEM and HRTEM image of single spiral nanorods, respectively. (g) FFT pattern from the image (f) and this is viewed along [10−1].

subsequent $CsPbBr_3$ nanorods. For the case of Cd(II), 15 min annealing was carried out to obtain yellow color solution; but in the second case with Pb(II), time dependent injections of parent nanorods were performed at different stages within 15 min period for obtaining different spiral nanorods. Figure 1a presents the schematic of the reaction where orthorhombic Cs_2CdBr_4 nanorods having [100] direction anisotropy was converted to the exciting [201] anisotropy of $CsPbBr_3$ nanorods. As shown, depending on the injection time, different shaped nanorods (A–D) were formed. Figure 1b presents the schematic atomic model resulting $CsPbBr_3$ nanorods in different conditions from A to D with variation of spirality. These models were designed as per obtained nanorods discussed in later section via spiral cutting of facets in the presence of mixture of ligands in different reaction stages. Ligand-I and Ligand-II marked in Figure 1a are the oleylammonium (primary ammonium) and the *N*,*N*-diphenacyl oleylammonium (tertiary ammonium) ions obtained

https://doi.org/10.1021/jacs.1c07231
J. Am. Chem. Soc. 2021, 143, 14895−14906

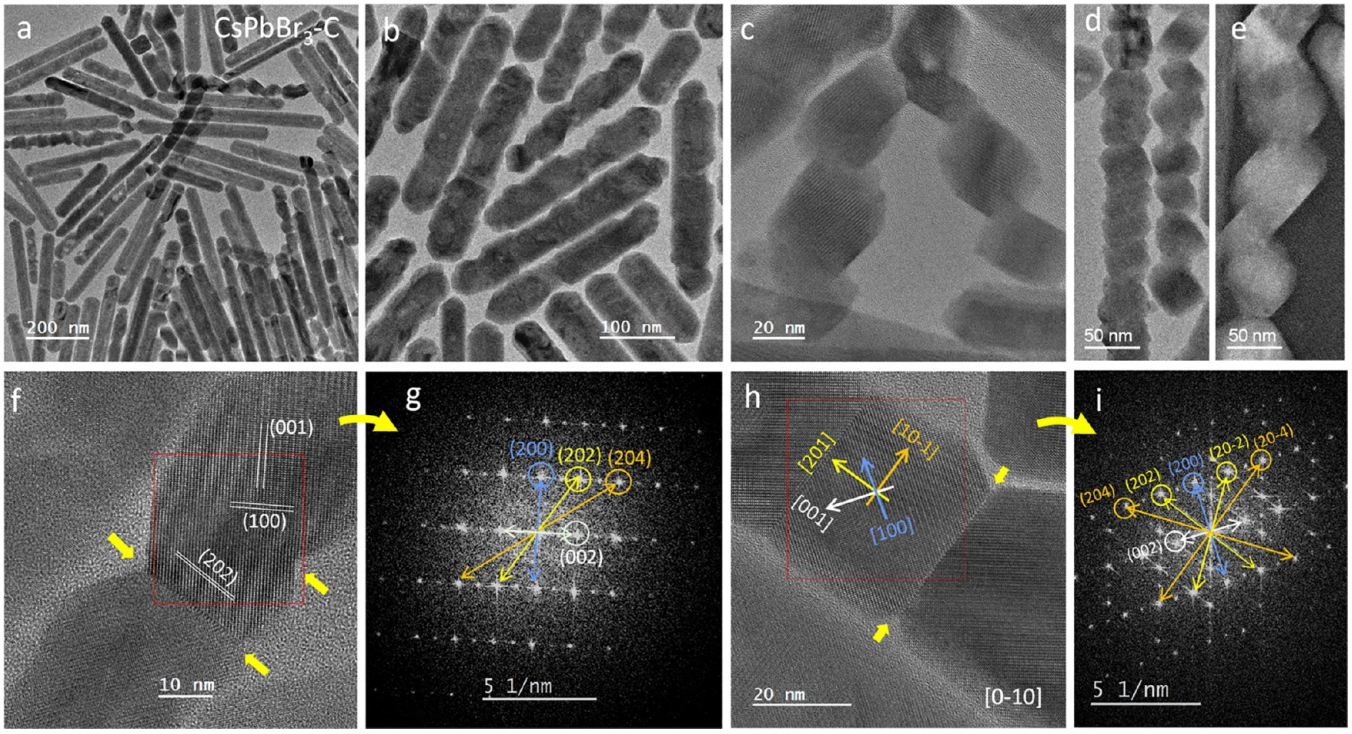

Figure 4. (a, b) TEM images of spiral $CsPbBr_3$ nanorods in different resolutions obtained from the reaction condition C of Figure 1. (c, d) Magnified TEM images and (e) inverted TEM image of spiral $CsPbBr_3$ nanorods. (f) HRTEM image of nanorod showing the junction obtained during spiral chemical cutting with ligands. (g) Selected area FFT pattern obtained from the HRTEM image (f). Planes are labeled and also marked in HRTEM image (f). (h) HRTEM image and (i) corresponding selected area FFT pattern of a different nanorod showing directions and plane orientations.

from the reaction of oleylamine with phenacyl bromide, respectively. In different stages from A to D, their compositions varied in the reaction system. More details of the synthesis process, change of colors during the reaction and also structure of ligands is presented in Figure S1 in the SI.

Figure 2a,b presents the inverted transmission electron microscopic (TEM) images of highly monodisperse Cs_2CdBr_4 nanorods (length ~220−250 nm) in different resolutions synthesized at 120 °C. More images of these nanorods are provided in Figures S2 and S3. Figure 2c presents the high-resolution TEM (HRTEM) image of these nanorods and its selected area fast Fourier transformed (FFT) pattern is shown in Figure 2d. Analysis suggested that these nanorods were in orthorhombic phase with the length direction [100] which was also further confirmed with the X-ray diffraction (XRD) pattern presented in later sections. It is worth mentioning here that the phenacyl bromide reagent was exclusive for obtaining such nanorods, else the widely reported benzoyl bromide led to hexagonal phase nanocrystals.[54] Even though there are reports on different compositions of Cs−Cd−Br with Pb,[53,64] but none led to orthorhombic rods with [100] anisotropy.

These obtained nanorods were further injected to the reaction mixture having Pb(II) and phenacyl bromide. Typically, with 15 min of annealing at 220 °C, the reaction mixture turned to yellow and this was further cooled down to 120 °C for the Cs_2CdBr_4 nanorod injection (condition A, Figure 1). Within a minute, these were converted to $CsPbBr_3$ nanorods retaining similar monodispersity. Under this reaction condition, the reaction system was expected to have predominantly the tertiary ammonium ion (Ligand-II, see the scheme in Figure 1). Figure 2e,f (see also Figure S4) presents inverted TEM images of the resulting $CsPbBr_3$ nanorods in different resolutions which were obtained from ~220−250 nm parent nanorods. From the image in Figure 2f, these rods were observed noncircular, rather faceted. Figure 2g presents the TEM image showing a vertically tilted rod and this suggested that these were truncated square or octagon like nanorods. Figure 2h presents a HRTEM image of this nanorod, and Figure 2i shows its selected area FFT pattern. Inter planner *d*-spacings of 0.58, 0.33, and 0.41 nm shown in FFT of Figure 2i suggested their planes as (002), (202), and (200), respectively, of the orthorhombic phase. Importantly, (202) planes in these nanorods remained nearly perpendicular to the major axis and as the phase is orthorhombic, the more appropriate viewing direction remained [201]. Accordingly, we assigned the anisotropic direction of these nanorods as [201].

Further, while parent Cs_2CdBr_4 nanorods were injected under the reaction condition B (Figure 1), where the mixture of Ligand-I and Ligand-II were expected in the reaction system, spiral nanorods were obtained. Figure 3a−c (more TEM images in Figures S5−S7) present the inverted TEM images of these nanorods in different resolutions confirming their spirality. Figure 3d presents the enlarged TEM image of these nanorods where the contrast differences also confirmed their spiral nature. Figure 3e,f presents the inverted TEM and HRTEM image of single spiral nanorods, respectively, where the spirality in each case was clearly visible. Selected area FFT pattern obtained from the HRTEM image of Figure 3f is shown in Figure 3g and analysis further confirmed the (202) planes remained perpendicular to the major axis of these nanorods. For clarity and visibility of the spirality, these parent nanorods intentionally took longer compared to the above presented nanorods by increasing their synthesis temperature.

https://doi.org/10.1021/jacs.1c07231
J. Am. Chem. Soc. 2021, 143, 14895−14906

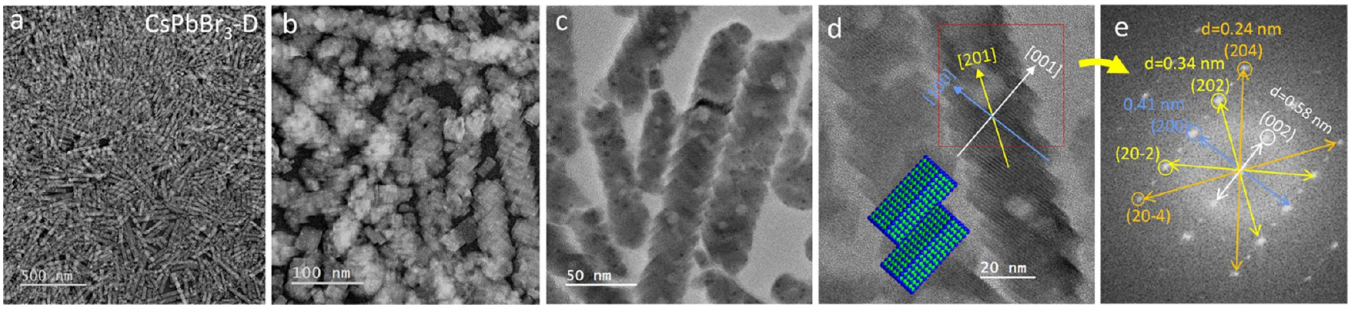

Figure 5. (a, b) Inverted TEM images of spiral $CsPbBr_3$ nanorods obtained under reaction condition D in different resolutions. (c) TEM and (d) HRTEM images of these spiral nanorods. (e) Selected area FFT pattern of the HRTEM of image in panel (d).

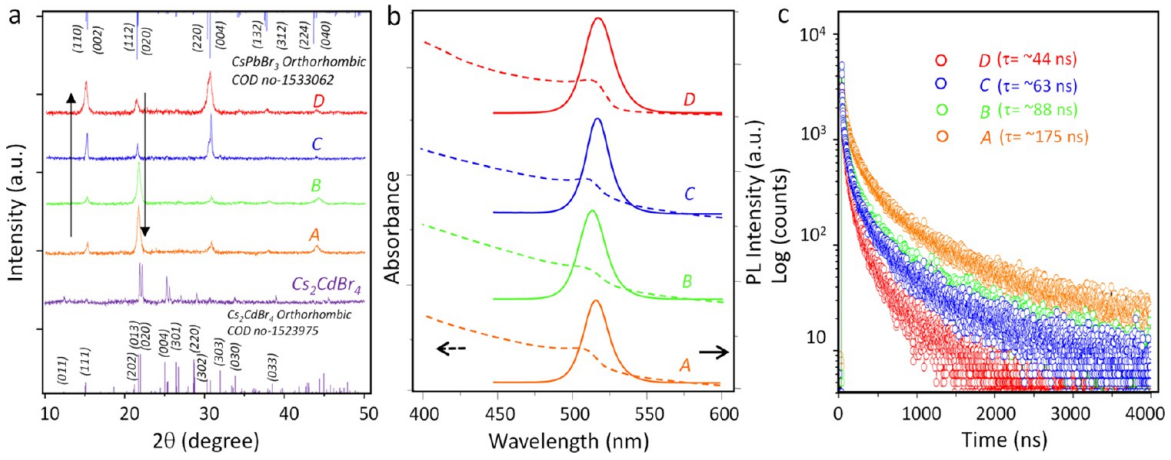

Figure 6. (a) XRD of Cs_2CdBr_4 and $CsPbBr_3$ nanorods obtained in different reaction conditions as stated in Figure 1. (b) Absorption and PL spectra of all four set of spiral nanorods (A to D). Excitation wavelength for the PL spectra remained 350 nm for all cases. (c) Excited state decay lifetime of all four spiral nanorods. In each panel nanorods of A to D are marked with colors for correlation.

To observe deeper spiral dissolution, the reaction was further carried out by injecting parent Cs_2CdBr_4 nanorods within 3 min to the reaction mixture (condition C, Figure 1). In this case, a mixture of Ligand-II and Ligand-I were also expected; but as the reaction time was shorter, the amount of Ligand-I was expected to be more than Ligand-II. Figure 4a,b (see also Figure S8) presents the TEM images of these obtained spiral nanorods in different resolutions.

TEM image in Figure 4a showed that some rods were not spiral, but the close-up view in Figure 4b confirmed that although it is to a lesser extent, almost all rods have some spirality. Figure 4c,d presents the magnified TEM images, and Figure 4e shows the color inverted TEM image of these nanorods. These images further confirmed the loss of more materials during the spirality in comparison to those nanorods shown in Figure 3. These look like the connected truncated nanocubes of $CsPbBr_3$. Figures 4f and S9 show HRTEM images of these nanorods confirming that their continuous skeleton and not the connection of preformed cubes. Figure 4g presents the selected area FFT pattern obtained from the HRTEM of Figure 4f, and the analysis also confirmed that (101) planes remained nearly perpendicular to the major axis. Yellow marks in the HRTEM signify different cutting junctions in these nanorods. Figure 4h shows another HRTEM image where junctions are clearly visible and its selected area FFT pattern is presented in Figure 4i. In this case, analyzed planes and corresponding directions also confirmed that these are the orthorhombic phase of $CsPbBr_3$ nanostructures and again their (101) planes (yellow line) remained perpendicular to the major axis. Other planes of (200), (204), and (002) are marked in the FFT and their perpendicular directions are shown in the corresponding HRTEM images.

Further reducing the injection time, Cs_2CdBr_4 nanorods were injected under the reaction condition D (Figure 1) where Ligand-I was expected to be predominant. This again led to deeper spirality and eliminated more facets of the parent nanorods. Figure 5a,b presents the inverted TEM images of these nanorods in different resolutions. More microscopic images are provided in Figure S10. Figure 5c represents a magnified TEM image confirming that the nanorods were spirally dissolved. These look-alike platelets were stacked in a regular manner forming nanorods though they were formed from parent nanorods. The HRTEM image in Figure 5d also confirmed a similar structure and a cartoon of model showing the stacking type of the platelets is also depicted in the inset. The selected area FFT pattern from this HRTEM is further depicted in Figure 5e. Planes corresponding to 0.41, 0.58, 0.34, and 0.24 nm represented the planes (200), (002), (202), and (204), respectively, of the orthorhombic $CsPbBr_3$. This also confirmed the same anisotropic direction as that discussed above for other perovskite nanorods.

As all these nanorods were obtained from Cs_2CdBr_4 parent nanorods and Cd(II) has the ability to form $CdBr_6^{4-}$ octahedra, these might also be retained in the $CsPbBr_3$ nanorods substituting Pb(II) positions. For the first round purification we have observed 1−3% Cd (Figure S11); but after the next round purification with ethyl acetate, the Cd(II) amount was drastically reduced (Figure S12) and hence, we

https://doi.org/10.1021/jacs.1c07231
J. Am. Chem. Soc. 2021, 143, 14895−14906

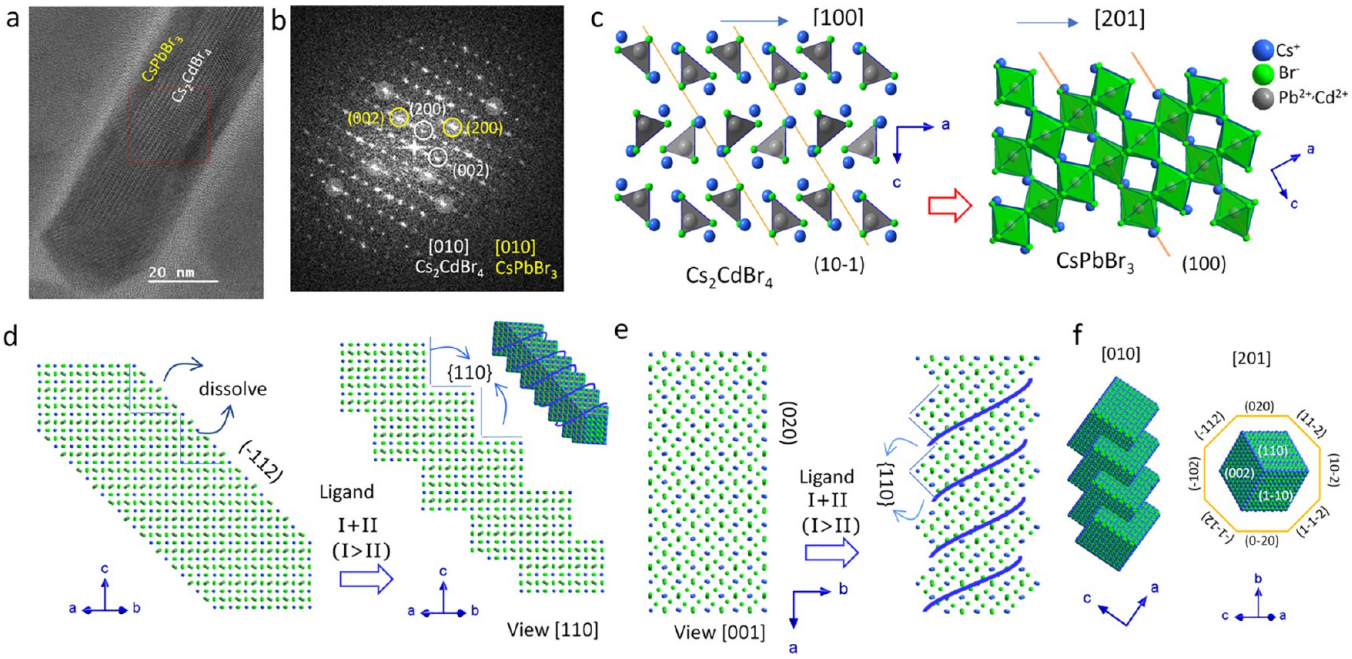

Figure 7. (a) HRTEM image and (b) corresponding selected area FFT pattern of an intermediate nanorod showing a junction of Cs_2CdBr_4 and $CsPbBr_3$. (c) Atomic model showing Cd-bromide tetrahedra and Pb-bromide octahedra in respective nanorods before and after the transformation. Viewing directions and alignments in this presentation were derived from the FFT pattern. (d) Schematic model showing spiral dissolution of facets with higher amounts of Ligand-I in comparison to Ligand-II condition. This was performed keeping the viewing direction [110]. Inset shows the space filled atomic model after the facet dissolutions. (e) Atomic models of nanorods presented with the viewing direction [001] and showing dissolution of {020} facets. (f) Atomic model showing a final spiral nanorod structure along [010] and [201] viewing directions after all such facet dissolutions.

could assume here that Cd(II) might be retained on the surfaces or their counts in energy dispersive spectra (EDS) appearing like contaminant. Hence, in all cases, we considered the nanorods as $CsPbBr_3$ and discuss them accordingly.

From all of the above four sets of reactions under conditions of A, B, C, and D, it is confirmed that all of these orthorhombic phase nanorods have (101) planes nearly perpendicular to the major axis. To further confirm this, XRD of all these samples including the parent Cs_2CdBr_4 nanorods are carried out and presented in Figure 6a. From diffraction peak positions, parent Cs_2CdBr_4 nanorods were confirmed orthorhombic phase and the intense peak of the (020) planes remained along the minor axis of the rod. However, the length was along [100] as confirmed in the HRTEM image. Further, after Pb(II) insertion, in all cases, the peaks closely resembled the widely reported orthorhombic phase of $CsPbBr_3$ nanostructures. Importantly, it was noticed that from condition A to D, intensities of (110) and (002) increase; but those of (112) and (020) decrease (shown in arrow marks in Figure 6a). This confirmed the change of structural configurations of these nanorods obtained from different reaction conditions. This also suggests that the polygonal nanorods slowly turned to cube/platelet connected type spiral nanorods.

For observing the optical characteristics, both absorption and photoluminescence (PL) spectra of all these nanorods were measured and presented in Figure 6b. In all cases, a green emission centered at ~518 nm was observed, though PL quantum yields (PLQY) varied from one to other. From the condition A, B, C, and D, the absolute PLQYs were observed as 30%, 46%, 51%, 62%, respectively (Figure S13) and this suggested that with deeper spirality or a more spiral cut, the better the PLQY became. However, importantly, even these showed excitonic emissions, but the decay lifetimes (Figure 6c and Table S1) were longer and varied from 175 to 44 ns in A to D.

For understanding the spirality obtained under different reaction conditions, details of the formation mechanisms are further investigated. As the entire study was originated from Cs_2CdBr_4 nanorods; at the beginning, the intermediate HRTEM image showing transformation of Cs_2CdBr_4 to $CsPbBr_3$ was analyzed. Figure 7a,b presents the HRTEM image and corresponding selected area FFT pattern of one of the intermediate nanorods. XRD, absorption, PL spectra, and EDS corresponding to these intermediate structures are provided in Figure S14. The HRTEM shows a clear distinguishing part of the core having Cs_2CdBr_4 and shell $CsPbBr_3$. From FFT, the *d*-spacing for planes perpendicular to the major axis was found to be 0.51 nm and that along the minor axis was 0.69 nm. These correspond to (200) and (002) planes of Cs_2CdBr_4. In addition, the *d*-spacings of 0.59 and 0.41 nm correspond to (002) and (200) planes of orthorhombic $CsPbBr_3$. As per the transformation, it can be assumed here that the anisotropic direction of the parent Cs_2CdBr_4 rod [100] turned to [201] of orthorhombic $CsPbBr_3$. Accordingly, atomic models for both Cs_2CdBr_4 and $CsPbBr_3$ are presented in Figure 7c keeping their alignments as those obtained from the HRTEM. This suggests that the unit partitioned with (101) planes (marked in Figure 7c) of Cs_2CdBr_4 transformed to the unit within two (200) planes of $CsPbBr_3$. Both crystal structures have the same viewing axis [010] and their *d*-spacings also match for (101)−(100) of orthorhombic Cs_2CdBr_4−$CsPbBr_3$ structures. Hence, such conversion was energetically favorable because this arrangement led to their minimum lattice transformation energy.

https://doi.org/10.1021/jacs.1c07231
J. Am. Chem. Soc. 2021, 143, 14895−14906

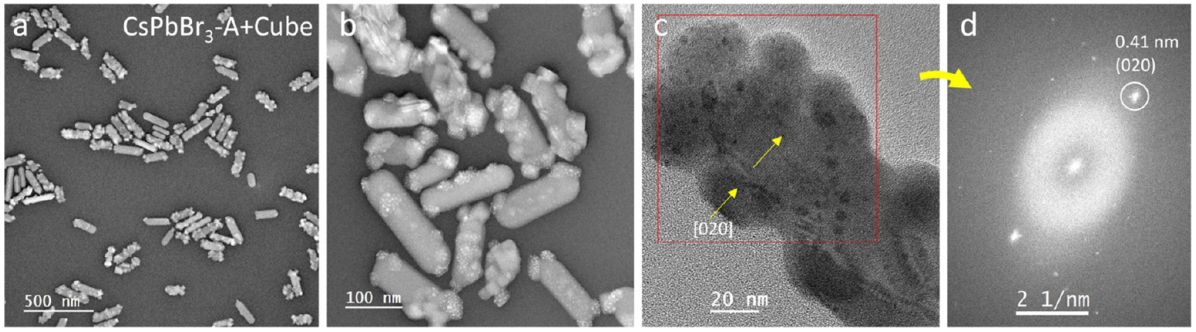

Figure 8. (a, b) Color inverted TEM images of cube decorated $CsPbBr_3$ nanorods in different resolutions obtained under reaction condition A; but with excess Cs(I) precursor. (c) HRTEM of this nanorod with epitaxially connected cube and (d) corresponding selected area FFT pattern.

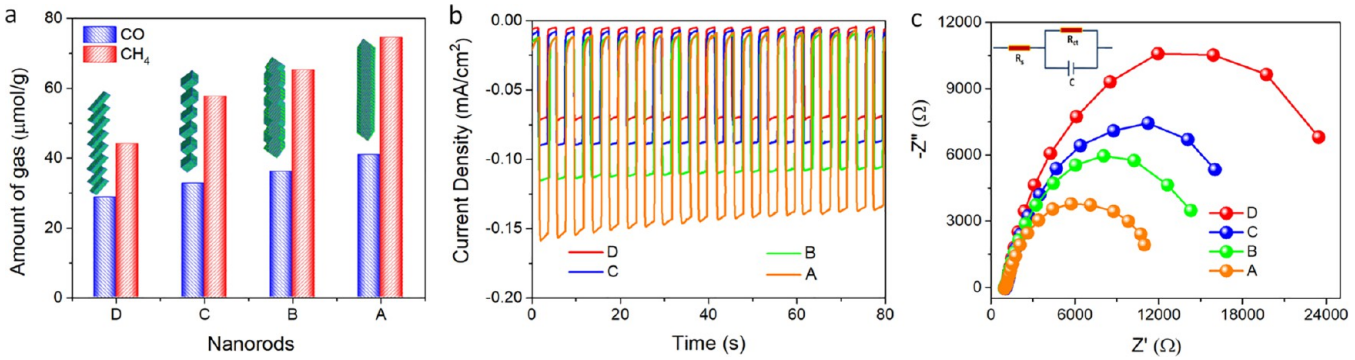

Figure 9. (a) Comparison of photocatalytic CO_2 reduction activity of four $CsPbBr_3$ nanorods. (b) Amperometric I-t plots measured at −0.4 V vs Ag/AgCl under 100 mW/cm^2 on−off illumination. (c) EIS (Nyquist plot) recorded under 100 mW/cm^2 continues illumination at −0.4 V vs Ag/AgCl, inset is the equivalent circuit model.

However, this matching was indeed privileged here for creating such unusual anisotropy which drove this unique spiral system.

To further understand the reaction conditions of Ligand-I and Ligand-II populations, the surface facets sustainability and dissolution of $CsPbBr_3$ are correlated. Primary oleylammonium bromide (Ligand-I) preferably stabilizes the six cubic facets (four 110 and two 002) having the planner *d*-spacing close to 0.58 nm.[65] However, the tertiary ammonium ions (Ligand-II) obtained from the reaction of oleylamine with phenacyl bromide dominantly stabilize {200} facets.[30,65] Hence, while the reaction condition varied from A to B and finally to C and D, Ligand-I populations gradually increased and this facilitated dissolutions of all other facets of the nanorods except {002} and {110} leading to spiral nanostructures. The presence of both Ligand-I and Ligand-II on the surface of spiral nanorods-B was further confirmed by ^{1}HNMR spectra, provided in Figure S15. Figure 7d presents the nanorod atomic model viewed along [110] where {112} facets were shown to be dissolved to some extent and retained the Ligand-I stabilized {110} facets. Inset picture on right side of Figure 7d already showed the initiation of spirality after such facet dissolution. Figure 7e presents the atomic model of the nanorod viewed along the [001] axis and here also, {010} facets were dissolved turning to {110} facets in each nanorod. Hence, all other facets except six facets of the standard nanocube while dissolved, this ultimately turned the final structure spiral. Figure 7f shows representative atomic models of a spiral nanorod created after such dissolutions with viewing directions [010] and [201]. The model viewed along [201] suggests that almost all facets ({112}, {020}, and {102}) of $CsPbBr_3$ nanorods were dissolved while the transformation progressed from A to D reaction system and retained only {110} and {002} facets.

The spiral cutting of facets were further seen intensified from A to D with an increase of Ligand-I population. Hence, the nature of the spiraling changed from one to another condition during the progress of the reaction. Even, rods obtained under condition B while treated again with condition C, the final rods attained to those as expected for C. As stated above, the most important part here is the anisotropic direction which was different from the standard *X*, *Y*, or *Z* axis expected for normal nanorods. As the orthorhombic phase has different atomic parameters, retained facets with increases in Ligand-I populations were not parallel to this major axis. Hence, the entire nanorod finally turned to become spirally connected truncated cubes or platelet-type structures. However, even these models show structures with regular intervals of dissolution, but practically this varied and under mixed ligands, these could show irregular spirality as observed in the images of Figures 3 and 4. Moreover, as these rods have symmetric atomic arrangements, the spiral directions should have been identical for all cases. However, in some cases, the presence of different orientations were observed even in one nanorod. A case is presented in Figure S16 where orientations of [100] and [001] axes were observed to be switched at a particular junction. This suggests that the spirality is either random or this needs more programmable reaction parameters to achieve identical spirality in each nanorod.

For extending the modulations of this synthesis, reaction parameters were further tuned and with an increase of Cs content under reaction condition A, coupled structures like half-cubes connected with $CsPbBr_3$ nanorods were observed.

https://doi.org/10.1021/jacs.1c07231
J. Am. Chem. Soc. 2021, 143, 14895−14906

Figure 8a,b presents the color inverted TEM images of these couple structures of nanorods where each rod was seen decorated with few cube-like structures. More TEM images and XRD confirming that all these materials are orthorhombic $CsPbBr_3$ are provided in Figures S17 and S18, respectively, in the SI. Figure 8c,d presents the HRTEM and corresponding selected area FFT pattern of a decorated nanorod. Analysis suggested that these nanocrystals were connected epitaxially on the surface of nanorods as they shared common {020} planes. It has been observed that half-cube like structures were also formed in Cs(I) rich conditions (see Figure S19) and these were connected to parent nanorods during annealing. The absorption and PL spectra of these nanostructures are shown in Figure S20. This is an example of modulations leading to new nanostructures and this confirmed perovskite nanocrystals even being ionic, facet dependent structural transformation could also be possible like that in covalent chalcogenide nanocrystal systems.

These four sets of nanorods (A−D) which showed variations of facets were further explored for CO_2 reduction to study their facet dependent adsorption ability in photocatalysis. Previously reported methods[66−68] of perovskite nanocrystal catalysts for CO_2 reduction in ethyl acetate medium were adopted for all these nanorods, and details of the procedure of catalytic measurements are provided in the Experimental Section. In all cases CH_4 was observed as the major product and its rate of evolution was related to the spiral nature of these nanorods. Figure 9a presents the histogram of the gaseous products obtained after 2 h of CO_2 photoreduction using all these nanorod samples. The output of the gaseous products generates linearly with prolonging reaction time (Figure S21). The superior catalytic activity was recorded for nanorod A followed by B, C, and D. The total yields of the obtained products were observed to be 115.26 μmol/g (74.45 μmol/g for CH_4 and 40.81 μmol/g for CO) for nanorod A than nanorod B (101.12 μmol/g), nanorod C (90.07 μmol/g), and nanorod D (72.59 μmol/g). These values are observed comparable to several other reports provided in Table S2. Post catalysis sample characterization is provided in Figures S22−S24 and show that there is no significant change in their morphology, phase, optical properties, and compositions.

The photoelectrochemical measurements also supported the above facts. The photoactivity of the prepared nanorods were evaluated through amperometric I-t measurements at a fixed potential of −0.4 V vs Ag/AgCl under chopped illumination of 100 mW/cm^2 and are presented in Figure 9b. From the result, it was evident that the maximum photocurrent density of 0.15 mA/cm^2 was observed for nanorod A and gradually decreased to 0.11 mA/cm^2 for nanorod B, 0.09 mA/cm^2 for nanorod C, and 0.07 mA/cm^2 for nanorod D. Therefore, nanorod A shows the greater photoactivity as reflected in their CO_2 reduction activity. In order to check the charge transfer activity during the photocatalytic reduction reaction, electrochemical impedance spectroscopy (EIS) measurements were carried out and the Nyquist plots were presented in Figure 9c. The diameter of the semicircle represents the charge transfer resistance at electrode−electrolyte interfaces. These semicircles were fitted with an equivalent circuit model (inset of Figure 9c) and the data are presented in Table S3. From Figure 9c, it was evident that the smallest semicircle was observed for nanorod A, suggesting the lowest charge transfer resistance (10.2 kΩ) and hence, enhanced catalytic activity. Upon spiralling of the nanorod, the charge transfer resistance also increased from 10.2 to 25.6 kΩ and thus, lowered the photocatalytic activity. From the above results, it can be concluded that with creation of {110} and {002} facets due to spiralling resulted in a decrease of adsorption of CO_2 and desorption of CH_4[66,69] and hence, while transforming from octagonal nanorods to spiral nanorods, the catalytic activity decreased. These results are just to support the importance of these materials and their successive facet dissolutions and evolutions. However, for more quantitative correlation, theoretical study is warranted for more understanding of the catalysis impact.

CONCLUSIONS

In conclusion, spiral $CsPbBr_3$ perovskite nanorods, unique among all kinds of solution processed 1D nanostructures, are reported. This spirality was induced by tuning the composition of surface ligands during reactions. This was possible by designing $CsPbBr_3$ nanorods with unusual anisotropic directions which with an increase of oleylammonium ions eliminated all facets other than its favorable {110} and {002} facets. As these facets did not align parallel to the major axis, the obtained nanorods turned into spiral-like structures. Synthesis of these anisotropic nanorods was made possible because of the retained lattice matching induced Pb(II) insertion in parent orthorhombic Cs_2CdBr_4 nanorods with eliminations of almost all Cd, turning to $CsPbBr_3$ nanorods. As these facets varied with varying spirality, these nanorods were further explored for catalysis in CO_2 reduction and change in the rate of catalysis was also observed with a change in the depth of spirality. Keeping this as a model, system extended modular synthesis leading to cube coupled nanorods was also fabricated. The above conclusions suggest that even perovskite nanocrystals are ionic and follow fast formation processes, but the shape could be modulated and new nanostructures could be synthesized. Moreover, while anisotropy is reported along [100] and [001] axes of orthorhombic $CsPbBr_3$, here addition of a [201] direction for nanorods further confirmed that designing perovskite nanostructures are versatile. They do not have any specific rules of anisotropy, but instead can be attained in any direction depending on the mode of their synthesis.

ASSOCIATED CONTENT

Supporting Information

The Supporting Information is available free of charge at https://pubs.acs.org/doi/10.1021/jacs.1c07231.

Details of synthesis scheme, additional TEMs of Cs_2CdBr_4, different spiral $CsPbBr_3$ nanorods, XRD, UV-PL, histogram of PLQY, parameters of decay lifetime plots, energy dispersive spectra, ^{1}HNMR, plots of gases obtained during catalysis with time measured in gas chromatography, electrochemical parameters of Nyquist plots, post catalysis samples TEM and XRD, and a comparison table (PDF)

AUTHOR INFORMATION

Corresponding Author

Narayan Pradhan − *School of Materials Sciences, Indian Association for the Cultivation of Science, Kolkata 700032, India;* orcid.org/0000-0003-4646-8488; Email: camnp@iacs.res.in

https://doi.org/10.1021/jacs.1c07231
J. Am. Chem. Soc. 2021, 143, 14895−14906

Authors

Suman Bera − *School of Materials Sciences, Indian Association for the Cultivation of Science, Kolkata 700032, India*

Sanjib Shyamal − *School of Materials Sciences, Indian Association for the Cultivation of Science, Kolkata 700032, India;* orcid.org/0000-0002-7255-506X

Complete contact information is available at: https://pubs.acs.org/10.1021/jacs.1c07231

Notes

The authors declare no competing financial interest.

■ ACKNOWLEDGMENTS

Capital grant of IACS is acknowledged for the purchase of the TEM (JEOL JEM F200). TRC at IACS and IACS faculty grants are acknowledged for their support with the consumables. S.B. acknowledges CSIR for the fellowship.

■ REFERENCES

(1) Protesescu, L.; Yakunin, S.; Bodnarchuk, M. I.; Krieg, F.; Caputo, R.; Hendon, C. H.; Yang, R. X.; Walsh, A.; Kovalenko, M. V. Nanocrystals of Cesium Lead Halide Perovskites ($CsPbX_3$, X = Cl, Br, and I): Novel Optoelectronic Materials Showing Bright Emission with Wide Color Gamut. *Nano Lett.* **2015**, *15*, 3692−3696.

(2) Akkerman, Q. A.; Raino, G.; Kovalenko, M. V.; Manna, L. Genesis, Challenges and Opportunities for Colloidal Lead Halide Perovskite Nanocrystals. *Nat. Mater.* **2018**, *17*, 394−405.

(3) Dey, A.; Ye, J.; De, A.; Debroye, E.; Ha, S. K.; Bladt, E.; Kshirsagar, A. S.; Wang, Z.; Yin, J.; Wang, Y.; et al. State of the Art and Prospects for Halide Perovskite Nanocrystals. *ACS Nano* **2021**, *15*, 10775−10981.

(4) Manser, J. S.; Christians, J. A.; Kamat, P. V. Intriguing Optoelectronic Properties of Metal Halide Perovskites. *Chem. Rev.* **2016**, *116*, 12956−13008.

(5) Huang, H.; Bodnarchuk, M. I.; Kershaw, S. V.; Kovalenko, M. V.; Rogach, A. L. Lead Halide Perovskite Nanocrystals in the Research Spotlight: Stability and Defect Tolerance. *ACS Energy Lett.* **2017**, *2*, 2071−2083.

(6) Pedesseau, L.; Sapori, D.; Traore, B.; Robles, R.; Fang, H.-H.; Loi, M. A.; Tsai, H.; Nie, W.; Blancon, J.-C.; Neukirch, A.; Tretiak, S.; Mohite, A. D.; Katan, C.; Even, J.; Kepenekian, M. Advances and Promises of Layered Halide Hybrid Perovskite Semiconductors. *ACS Nano* **2016**, *10*, 9776−9786.

(7) Zhou, Y.; Chen, J.; Bakr, O. M.; Sun, H.-T. Metal-Doped Lead Halide Perovskites: Synthesis, Properties, and Optoelectronic Applications. *Chem. Mater.* **2018**, *30*, 6589−6613.

(8) Shamsi, J.; Urban, A. S.; Imran, M.; De Trizio, L.; Manna, L. Metal Halide Perovskite Nanocrystals: Synthesis, Post-Synthesis Modifications, and Their Optical Properties. *Chem. Rev.* **2019**, *119*, 3296−3348.

(9) Kazes, M.; Udayabhaskararao, T.; Dey, S.; Oron, D. Effect of Surface Ligands in Perovskite Nanocrystals: Extending in and Reaching out. *Acc. Chem. Res.* **2021**, *54*, 1409−1418.

(10) Smock, S. R.; Chen, Y.; Rossini, A. J.; Brutchey, R. L. The Surface Chemistry and Structure of Colloidal Lead Halide Perovskite Nanocrystals. *Acc. Chem. Res.* **2021**, *54*, 707−718.

(11) Zhang, Q.; Yin, Y. All-Inorganic Metal Halide Perovskite Nanocrystals: Opportunities and Challenges. *ACS Cent. Sci.* **2018**, *4*, 668−679.

(12) Bera, S.; Pradhan, N. Perovskite Nanocrystal Heterostructures: Synthesis, Optical Properties, and Applications. *ACS Energy Lett.* **2020**, *5*, 2858−2872.

(13) Ha, S.-T.; Su, R.; Xing, J.; Zhang, Q.; Xiong, Q. Metal Halide Perovskite Nanomaterials: Synthesis and Applications. *Chem. Sci.* **2017**, *8*, 2522−2536.

(14) Liu, Z.; Bekenstein, Y.; Ye, X.; Nguyen, S. C.; Swabeck, J.; Zhang, D.; Lee, S.-T.; Yang, P.; Ma, W.; Alivisatos, A. P. Ligand Mediated Transformation of Cesium Lead Bromide Perovskite Nanocrystals to Lead Depleted Cs_4PbBr_6 Nanocrystals. *J. Am. Chem. Soc.* **2017**, *139*, 5309−5312.

(15) Pan, J.; Shang, Y.; Yin, J.; De Bastiani, M.; Peng, W.; Dursun, I.; Sinatra, L.; El-Zohry, A. M.; Hedhili, M. N.; Emwas, A.-H.; Mohammed, O. F.; Ning, Z.; Bakr, O. M. Bidentate Ligand-Passivated $CsPbI_3$ Perovskite Nanocrystals for Stable Near-Unity Photoluminescence Quantum Yield and Efficient Red Light-Emitting Diodes. *J. Am. Chem. Soc.* **2018**, *140*, 562−565.

(16) Pradhan, N. Journey of Making Cesium Lead Halide Perovskite Nanocrystals: What's Next. *J. Phys. Chem. Lett.* **2019**, *10*, 5847−5855.

(17) Huang, H.; Polavarapu, L.; Sichert, J. A.; Susha, A. S.; Urban, A. S.; Rogach, A. L. Colloidal Lead Halide Perovskite Nanocrystals: Synthesis, Optical Properties and Applications. *NPG Asia Mater.* **2016**, *8*, No. e328.

(18) Almeida, G.; Infante, I.; Manna, L. Resurfacing Halide Perovskite Nanocrystals. *Science* **2019**, *364*, 833−834.

(19) Kovalenko, M. V.; Protesescu, L.; Bodnarchuk, M. I. Properties and Potential Optoelectronic Applications of Lead Halide Perovskite Nanocrystals. *Science* **2017**, *358*, 745−750.

(20) Zhang, B.; Goldoni, L.; Lambruschini, C.; Moni, L.; Imran, M.; Pianetti, A.; Pinchetti, V.; Brovelli, S.; De Trizio, L.; Manna, L. Stable and Size Tunable $CsPbBr_3$ Nanocrystals Synthesized with Oleylphosphonic Acid. *Nano Lett.* **2020**, *20*, 8847−8853.

(21) Brown, A. A. M.; Vashishtha, P.; Hooper, T. J. N.; Ng, Y. F.; Nutan, G. V.; Fang, Y.; Giovanni, D.; Tey, J. N.; Jiang, L.; Damodaran, B.; Sum, T. C.; Pu, S. H.; Mhaisalkar, S. G.; Mathews, N. Precise Control of $CsPbBr_3$ Perovskite Nanocrystal Growth at Room Temperature: Size Tunability and Synthetic Insights. *Chem. Mater.* **2021**, *33*, 2387−2397.

(22) Wen, J.-R.; Roman, B. J.; Rodriguez Ortiz, F. A.; Mireles Villegas, N.; Porcellino, N.; Sheldon, M. Chemical Availability of Bromide Dictates $CsPbBr_3$ Nanocrystal Growth. *Chem. Mater.* **2019**, *31*, 8551−8557.

(23) Dong, H.; Zhang, C.; Liu, X.; Yao, J.; Zhao, Y. S. Materials Chemistry and Engineering in Metal Halide Perovskite Lasers. *Chem. Soc. Rev.* **2020**, *49*, 951−982.

(24) Fu, Y.; Zhu, H.; Chen, J.; Hautzinger, M. P.; Zhu, X. Y.; Jin, S. Metal Halide Perovskite Nanostructures for Optoelectronic Applications and the Study of Physical Properties. *Nat. Rev. Mater.* **2019**, *4*, 169−188.

(25) Imran, M.; Caligiuri, V.; Wang, M.; Goldoni, L.; Prato, M.; Krahne, R.; De Trizio, L.; Manna, L. Benzoyl Halides as Alternative Precursors for the Colloidal Synthesis of Lead-Based Halide Perovskite Nanocrystals. *J. Am. Chem. Soc.* **2018**, *140*, 2656−2664.

(26) Paul, S.; Samanta, A. N-Bromosuccinimide as Bromide Precursor for Direct Synthesis of Stable and Highly Luminescent Green-Emitting Perovskite Nanocrystals. *ACS Energy Lett.* **2020**, *5*, 64−69.

(27) Dutta, A.; Dutta, S. K.; Das Adhikari, S.; Pradhan, N. Tuning the Size of $CsPbBr_3$ Nanocrystals: All at One Constant Temperature. *ACS Energy Lett.* **2018**, *3*, 329−334.

(28) Xu, L.-J.; Worku, M.; He, Q.; Lin, H.; Zhou, C.; Chen, B.; Lin, X.; Xin, Y.; Ma, B. Ligand-Mediated Release of Halides for Color Tuning of Perovskite Nanocrystals with Enhanced Stability. *J. Phys. Chem. Lett.* **2019**, *10*, 5836−5840.

(29) Creutz, S. E.; Crites, E. N.; De Siena, M. C.; Gamelin, D. R. Anion Exchange in Cesium Lead Halide Perovskite Nanocrystals and Thin Films Using Trimethylsilyl Halide Reagents. *Chem. Mater.* **2018**, *30*, 4887−4891.

(30) Bera, S.; Behera, R. K.; Pradhan, N. α-Halo Ketone for Polyhedral Perovskite Nanocrystals: Evolutions, Shape Conversions, Ligand Chemistry, and Self-Assembly. *J. Am. Chem. Soc.* **2020**, *142*, 20865−20874.

(31) Krieg, F.; Ochsenbein, S. T.; Yakunin, S.; ten Brinck, S.; Aellen, P.; Suess, A.; Clerc, B.; Guggisberg, D.; Nazarenko, O.; Shynkarenko, Y.; Kumar, S.; Shih, C.-J.; Infante, I.; Kovalenko, M. V. Colloidal $CsPbX_3$ (X = Cl, Br, I) Nanocrystals 2.0: Zwitterionic Capping

Ligands for Improved Durability and Stability. *ACS Energy Lett.* **2018**, *3*, 641−646.
(32) Dirin, D. N.; Dreyfuss, S.; Bodnarchuk, M. I.; Nedelcu, G.; Papagiorgis, P.; Itskos, G.; Kovalenko, M. V. Lead Halide Perovskites and Other Metal Halide Complexes As Inorganic Capping Ligands for Colloidal Nanocrystals. *J. Am. Chem. Soc.* **2014**, *136*, 6550−6553.
(33) Gratzel, M. The Rise of Highly Efficient and Stable Perovskite Solar Cells. *Acc. Chem. Res.* **2017**, *50*, 487−491.
(34) Sheikh, T.; Maqbool, S.; Mandal, P.; Nag, A. Introducing Intermolecular Cation-π Interactions for Water-Stable Low Dimensional Hybrid Lead Halide Perovskites. *Angew. Chem., Int. Ed.* **2021**, *60*, 18265−18271.
(35) Quarta, D.; Imran, M.; Capodilupo, A.-L.; Petralanda, U.; van Beek, B.; De Angelis, F.; Manna, L.; Infante, I.; De Trizio, L.; Giansante, C. Stable Ligand Coordination at the Surface of Colloidal $CsPbBr_3$ Nanocrystals. *J. Phys. Chem. Lett.* **2019**, *10*, 3715−3726.
(36) Cohen, T. A.; Huang, Y.; Bricker, N. A.; Juhl, C. S.; Milstein, T. J.; MacKenzie, J. D.; Luscombe, C. K.; Gamelin, D. R. Modular Zwitterion-Functionalized Poly(isopropyl methacrylate) Polymers for Hosting Luminescent Lead Halide Perovskite Nanocrystals. *Chem. Mater.* **2021**, *33*, 3779−3790.
(37) Krieg, F.; Ong, Q. K.; Burian, M.; Rainò, G.; Naumenko, D.; Amenitsch, H.; Süess, A.; Grotevent, M. J.; Krumeich, F.; Bodnarchuk, M. I.; Shorubalko, I.; Stellacci, F.; Kovalenko, M. V. Stable Ultraconcentrated and Ultradilute Colloids of $CsPbX_3$ (X = Cl, Br) Nanocrystals Using Natural Lecithin as a Capping Ligand. *J. Am. Chem. Soc.* **2019**, *141*, 19839−19849.
(38) Hills-Kimball, K.; Yang, H.; Cai, T.; Wang, J.; Chen, O. Recent Advances in Ligand Design and Engineering in Lead Halide Perovskite Nanocrystals. *Adv. Sci.* **2021**, *8*, 2100214.
(39) Zheng, X.; Hou, Y.; Sun, H.-T.; Mohammed, O. F.; Sargent, E. H.; Bakr, O. M. Reducing Defects in Halide Perovskite Nanocrystals for Light-Emitting Applications. *J. Phys. Chem. Lett.* **2019**, *10*, 2629−2640.
(40) Pradhan, N. Tips and Twists in Making High Photoluminescence Quantum Yield Perovskite Nanocrystals. *ACS Energy Lett.* **2019**, *4*, 1634−1638.
(41) Seth, S.; Ahmed, T.; De, A.; Samanta, A. Tackling the Defects, Stability, and Photoluminescence of $CsPbX_3$ Perovskite Nanocrystals. *ACS Energy Lett.* **2019**, *4*, 1610−1618.
(42) Ahmed, T.; Seth, S.; Samanta, A. Boosting the Photoluminescence of $CsPbX_3$ (X = Cl, Br, I) Perovskite Nanocrystals Covering a Wide Wavelength Range by Postsynthetic Treatment with Tetrafluoroborate Salts. *Chem. Mater.* **2018**, *30*, 3633−3637.
(43) Almeida, G.; Goldoni, L.; Akkerman, Q.; Dang, Z.; Khan, A. H.; Marras, S.; Moreels, I.; Manna, L. Role of Acid−Base Equilibria in the Size, Shape, and Phase Control of Cesium Lead Bromide Nanocrystals. *ACS Nano* **2018**, *12*, 1704−1711.
(44) Zhang, Y.; Siegler, T. D.; Thomas, C. J.; Abney, M. K.; Shah, T.; De Gorostiza, A.; Greene, R. M.; Korgel, B. A. A "Tips and Tricks" Practical Guide to the Synthesis of Metal Halide Perovskite Nanocrystals. *Chem. Mater.* **2020**, *32*, 5410−5423.
(45) Li, J.; Zhang, H.; Wang, S.; Long, D.; Li, M.; Wang, D.; Zhang, T. Inter-Conversion between Different Compounds of Ternary Cs-Pb-Br System. *Materials* **2018**, *11*, 717.
(46) Palazon, F.; Urso, C.; De Trizio, L.; Akkerman, Q.; Marras, S.; Locardi, F.; Nelli, I.; Ferretti, M.; Prato, M.; Manna, L. Postsynthesis Transformation of Insulating Cs_4PbBr_6 Nanocrystals into Bright Perovskite $CsPbBr_3$ through Physical and Chemical Extraction of CsBr. *ACS Energy Lett.* **2017**, *2*, 2445−2448.
(47) Yang, H.; Zhang, Y.; Pan, J.; Yin, J.; Bakr, O. M.; Mohammed, O. F. Room-Temperature Engineering of All-Inorganic Perovskite Nanocrystals with Different Dimensionalities. *Chem. Mater.* **2017**, *29*, 8978−8982.
(48) Toso, S.; Baranov, D.; Manna, L. Hidden in Plain Sight: The Overlooked Influence of the Cs^+ Substructure on Transformations in Cesium Lead Halide Nanocrystals. *ACS Energy Lett.* **2020**, *5*, 3409−3414.
(49) Shamsi, J.; Dang, Z.; Ijaz, P.; Abdelhady, A. L.; Bertoni, G.; Moreels, I.; Manna, L. Colloidal CsX (X = Cl, Br, I) Nanocrystals and Their Transformation to $CsPbX_3$ Nanocrystals by Cation Exchange. *Chem. Mater.* **2018**, *30*, 79−83.
(50) Hudait, B.; Dutta, S. K.; Bera, S.; Pradhan, N. Introducing B-Site Cations by Ion Exchange and Shape Anisotropy in $CsPbBr_3$ Perovskite Nanostructures. *Nano Lett.* **2021**, *21*, 5277−5284.
(51) Roccanova, R.; Ming, W.; Whiteside, V. R.; McGuire, M. A.; Sellers, I. R.; Du, M.-H.; Saparov, B. Synthesis, Crystal and Electronic Structures, and Optical Properties of $(CH_3NH_3)_2CdX_4$ (X = Cl, Br, I). *Inorg. Chem.* **2017**, *56*, 13878−13888.
(52) van der Stam, W.; Geuchies, J. J.; Altantzis, T.; van den Bos, K. H. W.; Meeldijk, J. D.; Van Aert, S.; Bals, S.; Vanmaekelbergh, D.; de Mello Donega, C. Highly Emissive Divalent-Ion-Doped Colloidal $CsPb_{1-x}M_xBr_3$ Perovskite Nanocrystals through Cation Exchange. *J. Am. Chem. Soc.* **2017**, *139*, 4087−4097.
(53) Guo, J.; Fu, Y.; Lu, M.; Zhang, X.; Kershaw, S. V.; Zhang, J.; Luo, S.; Li, Y.; Yu, W. W.; Rogach, A. L.; Zhang, L.; Bai, X. Cd-Rich Alloyed $CsPb_{1-x}Cd_xBr_3$ Perovskite Nanorods with Tunable Blue Emission and Fermi Levels Fabricated through Crystal Phase Engineering. *Adv. Sci.* **2020**, *7*, 2000930.
(54) Imran, M.; Ramade, J.; Di Stasio, F.; De Franco, M.; Buha, J.; Van Aert, S.; Goldoni, L.; Lauciello, S.; Prato, M.; Infante, I.; Bals, S.; Manna, L. Alloy $CsCd_xPb_{1-x}Br_3$ Perovskite Nanocrystals: The Role of Surface Passivation in Preserving Composition and Blue Emission. *Chem. Mater.* **2020**, *32*, 10641−10652.
(55) Bekenstein, Y.; Koscher, B. A.; Eaton, S. W.; Yang, P.; Alivisatos, A. P. Highly Luminescent Colloidal Nanoplates of Perovskite Cesium Lead Halide and Their Oriented Assemblies. *J. Am. Chem. Soc.* **2015**, *137*, 16008−16011.
(56) Zhang, D.; Eaton, S. W.; Yu, Y.; Dou, L.; Yang, P. Solution-Phase Synthesis of Cesium Lead Halide Perovskite Nanowires. *J. Am. Chem. Soc.* **2015**, *137*, 9230−9233.
(57) Imran, M.; Di Stasio, F.; Dang, Z.; Canale, C.; Khan, A. H.; Shamsi, J.; Brescia, R.; Prato, M.; Manna, L. Colloidal Synthesis of Strongly Fluorescent $CsPbBr_3$ Nanowires with Width Tunable down to the Quantum Confinement Regime. *Chem. Mater.* **2016**, *28*, 6450−6454.
(58) Jing, Q.; Su, Y.; Xing, X.; Lu, Z. Highly Luminescent $CsPbBr_3$ Nanorods Synthesized by a Ligand-Regulated Reaction at the Water−Oil Interface. *J. Mater. Chem. C* **2019**, *7*, 1854−1858.
(59) Chakrabarty, A.; Satija, S.; Gangwar, U.; Sapra, S. Precursor-Mediated Synthesis of Shape-Controlled Colloidal $CsPbBr_3$ Perovskite Nanocrystals and Their Nanofiber-Directed Self-Assembly. *Chem. Mater.* **2020**, *32*, 721−733.
(60) Liu, J.; Song, K.; Shin, Y.; Liu, X.; Chen, J.; Yao, K. X.; Pan, J.; Yang, C.; Yin, J.; Xu, L.-J.; Yang, H.; El-Zohry, A. M.; Xin, B.; Mitra, S.; Hedhili, M. N.; Roqan, I. S.; Mohammed, O. F.; Han, Y.; Bakr, O. M. Light-Induced Self-Assembly of Cubic $CsPbBr_3$ Perovskite Nanocrystals into Nanowires. *Chem. Mater.* **2019**, *31*, 6642−6649.
(61) Yang, D.; Li, P.; Zou, Y.; Cao, M.; Hu, H.; Zhong, Q.; Hu, J.; Sun, B.; Duhm, S.; Xu, Y.; Zhang, Q. Interfacial Synthesis of Monodisperse $CsPbBr_3$ Nanorods with Tunable Aspect Ratio and Clean Surface for Efficient Light-Emitting Diode Applications. *Chem. Mater.* **2019**, *31*, 1575−1583.
(62) Wang, S.; Yu, J.; Zhang, M.; Chen, D.; Li, C.; Chen, R.; Jia, G.; Rogach, A. L.; Yang, X. Stable, Strongly Emitting Cesium Lead Bromide Perovskite Nanorods with High Optical Gain Enabled by an Intermediate Monomer Reservoir Synthetic Strategy. *Nano Lett.* **2019**, *19*, 6315−6322.
(63) Rao, L.; Tang, Y.; Song, C.; Xu, K.; Vickers, E. T.; Bonabi Naghadeh, S.; Ding, X.; Li, Z.; Zhang, J. Z. Polar-Solvent-Free Synthesis of Highly Photoluminescent and Stable $CsPbBr_3$ Nanocrystals with Controlled Shape and Size by Ultrasonication. *Chem. Mater.* **2019**, *31*, 365−375.
(64) Guo, J.; Hu, Q.; Lu, M.; Li, A.; Zhang, X.; Sheng, R.; Chen, P.; Zhang, Y.; Wu, J.; Fu, Y.; Sun, G.; Yu, W. W.; Bai, X. Pb^{2+} Doped $CsCdBr_3$ Perovskite Nanorods for Pure-Blue Light-Emitting Diodes. *Chem. Eng. J.* **2022**, *427*, 131010.

https://doi.org/10.1021/jacs.1c07231
J. Am. Chem. Soc. 2021, 143, 14895−14906

(65) Pradhan, N. Why Do Perovskite Nanocrystals Form Nanocubes and How Can Their Facets Be Tuned? A Perspective from Synthetic Prospects. *ACS Energy Lett.* **2021**, *6*, 92−99.
(66) Shyamal, S.; Dutta, S. K.; Das, T.; Sen, S.; Chakraborty, S.; Pradhan, N. Facets and Defects in Perovskite Nanocrystals for Photocatalytic CO_2 Reduction. *J. Phys. Chem. Lett.* **2020**, *11*, 3608−3614.
(67) Shyamal, S.; Dutta, S. K.; Pradhan, N. Doping Iron in $CsPbBr_3$ Perovskite Nanocrystals for Efficient and Product Selective CO_2 Reduction. *J. Phys. Chem. Lett.* **2019**, *10*, 7965−7969.
(68) Xu, Y.-F.; Yang, M.-Z.; Chen, B.-X.; Wang, X.-D.; Chen, H.-Y.; Kuang, D.-B.; Su, C.-Y. A $CsPbBr_3$ Perovskite Quantum Dot/Graphene Oxide Composite for Photocatalytic CO_2 Reduction. *J. Am. Chem. Soc.* **2017**, *139*, 5660−5663.
(69) Zhang, Z.; Jiang, Y.; Shu, M.; Li, L.; Dong, Z.; Xu, J. Artificial Photosynthesis over Metal Halide Perovskites: Achievements, Challenges, and Prospects. *J. Phys. Chem. Lett.* **2021**, *12*, 5864−5870.

https://doi.org/10.1021/jacs.1c07231
J. Am. Chem. Soc. 2021, 143, 14895−14906